View metadata, citation and similar papers at core.ac.uk

brought to you by CORE

provided by Chalmers Research

Comparison of Steering Feel Control Strategies in Electric Power Assisted Steering

Downloaded from: https://research.chalmers.se, 2019-11-13 13:40 UTC

Citation for the original published paper (version of record):

Chugh, T., Bruzelius, F., Klomp, M. et al (2018)
Comparison of Steering Feel Control Strategies in Electric Power Assisted Steering
International Symposium on Advanced Vehicle Control

N.B. When citing this work, cite the original published paper.

research.chalmers.se offers the possibility of retrieving research publications produced at Chalmers University of Technology.
It covers all kind of research output: articles, dissertations, conference papers, reports etc. since 2004.
research.chalmers.se is administrated and maintained by Chalmers Library

(article starts on next page)

Comparison of Steering Feel Control Strategies in Electric Power Assisted Steering

Tushar Chugh[*+], Fredrik Bruzelius[+#], Matthijs Klomp[*+], Shenhai Ran[*]
[*]Volvo Cars, [+]Chalmers University of Technology,
[#]Swedish National Road and Transport Research Institute (VTI)
E-mail: tushar.chugh@volvocars.com

This paper presents an objective comparison of two closed-loop steering feel control concepts in an electric power assisted steering (EPAS) system. The closed-loop methods, torque- and position-control, aim to compensate the EPAS motor inertia in an effective manner as compared to the open loop (feed-forward) solution. For a given steering feel reference, the feedback controllers are developed in a sequential manner ensuring coupled stability. Linear system theory is used for the analysis. For a comparable reference tracking and stability margin, higher haptic controller bandwidth is achieved in torque-control. The position controller stability and performance are limited due to feedback control filtering and high system inertia (from EPAS motor and driver arms), which further makes it more sensitive towards muscle co-contraction. Moreover, torque-control offers better road disturbance attenuation for low and high frequency spectrum, whereas position-control is better for mid-frequency range.

Topics/ Vehicle Dynamics and Chassis Control, Advanced Driver Assistant Systems, Haptic Feedback Control

1 INTRODUCTION

In a typical mechanical-assisted system, the motor inertia contributes to an additional impedance. Due to this shortcoming, the system bandwidth is reduced as compared to its passive characteristic. Without compensating the additional impedance, the high frequency tracking or system dynamics is compromised [1]. This is in analogy for the system under consideration, rack mounted electric power assisted steering (EPAS) system. The effect is further amplified by the mechanical gear ratio between the electric motor and steering hardware, see [2, 3]. Subsequently, it results in a fundamental difference to the passive response (or high bandwidth) of the hydraulic assisted system.

The straightforward EPAS control method is open loop. Various feed-forward functions including non-linear basic assist, inertia compensation, active damping, etc. are implemented to fulfill the purpose of a good steering feel, refer [4, 2]. The aim is to replicate the hydraulic assisted system. This is achieved typically for lower frequencies, but the dynamics is affected due to the above mentioned reason. The potential of feed-forward inertia compensation is limited due to model uncertainties [5]. As a result, the measurement noise might get amplified during the differentiation and can raise stability concerns especially for high impedance. The foremost motivation of compensating the EPAS motor inertia by developing a closed-loop approach is investigated in this paper.

The closed-loop approach have two distinct variants depending on the feedback control variable; torque or position/velocity. Position- and velocity-control are considered under the same category of controlling the motion state. Torque- and position-control methods are in a sense inverse to each other. For reference position, torque disturbance is required and position disturbance for torque reference. The research on haptic controllers has been done for mechanical systems where the actuator interacts directly with the human, see [1, 6]. For EPAS systems, there is a mechanical connection between the state variables; rack position and steering angle (which is different than disconnected systems, e.g. Steer-by-Wire). Although there are examples of EPAS closed-loop steering feel controllers as discussed in [7, 3], but there is no objective comparison between the two methods in the existing literature. Therefore, the differences in tracking performance, stability and disturbance attenuation for the two approaches are studied in this paper. With a closed-loop solution, the controller can decouple the system from the external load disturbance (originating from the environment). Similarly, the closed-loop steering feel controller attenuates the road disturbance and generates a feedback based on the reference generator.

Besides steering feel, the control algorithm should incorporate the external intervention from lateral vehicle control (active safety) functions. These functions, such as Lane Keeping Aid, Pilot Assist [8], etc. increase the vehicle automation level. They aim to maintain the reference vehicle position; and the suitable control variable is steering rack position. In an open loop architecture, these functions could be in isolation to the steering feel functionality and merged at the motor torque request similar to [4]. For driver acceptance, it is crucial that the intervention is perceived consistent and intuitive. Hence, the external intervention is realized via the proposed steering feel controllers.

As a first step, the controllers are designed with classical control theory. A driver model is necessary to develop a stable human coupled interaction. With a defined stability margin, the reference tracking is evaluated. In this regard, a fixed steering feel reference at a given vehicle speed is based on virtual dynamics considering the driver excitation. The closed-loop controllers attenuate the road disturbances and mimic the virtual dynamics. The paper focuses on the feedback control and therefore, the road feedback content is not considered in the reference for a simplified analysis. The comparison is done in classical measures of bandwidth, loop gain phase margin, etc. Finally using the same control law (from reference tracking), road disturbance attenuation and external intervention are briefly discussed.

2 SYSTEM DYNAMICS

This section introduces an overview of the implemented mechanical models, steering feel reference generator and system identification scheme for steering rack parameter estimation.

2.1 EPAS and Driver Model

In an EPAS system, the interaction of the motor with the driver is not completely direct due to the mechanical connection with the

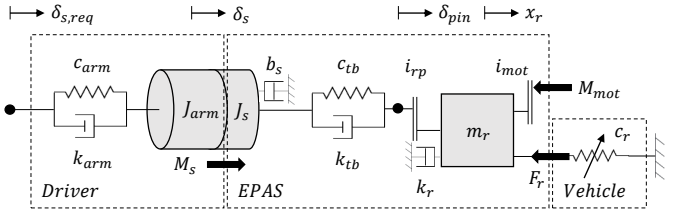

Figure 1: Block diagram of EPAS and driver mechanical model. The single-track vehicle model is not shown (applying rack force, F_r) instead it is represented by a spring, c_r. EPAS motor torque (M_{mot}) translates to rack assist force by gear ratio i_{mot}.

road. The steering torque, M_s, translates to the steering rack via torsion bar compliance (c_{tb}, k_{tb}), refer Fig. 1 and (1)−(3). Pinion angle (δ_{pin}) is mechanically constrained to rack position (x_r), such that $\delta_{pin} = i_{rp} x_r$. Equation (1) and (2) represent the force balance on the steering wheel and rack respectively. The front axle lateral tire force generating the rack force, F_r, is obtained from the single-track vehicle model, see [9]. Coulomb friction is not considered for the controller development assuming high amplitude excitations within sliding friction regime.

$$(J_s + J_{arm})\ddot{\delta}_s(t) + b_s\dot{\delta}_s(t) = M_s(t) - M_{tb}(t) \quad (1)$$

$$m_r\ddot{x}_r(t) + k_r\dot{x}_r(t) = M_{tb}(t)\, i_{rp} + M_{mot}(t)\, i_{mot} - F_r(t) \quad (2)$$

$$k_{tb}(\dot{\delta}_s(t) - \dot{\delta}_{pin}(t)) + c_{tb}(\delta_s(t) - \delta_{pin}(t)) = M_{tb}(t) \quad (3)$$

$$k_{arm}(\dot{\delta}_{s,req}(t) - \dot{\delta}_s(t)) + c_{arm}(\delta_{s,req}(t) - \delta_s(t)) = M_s(t) \quad (4)$$

The driver model is a second-order system. This simplified model is easy to analyze coupled stability, further discussed in section 3. The arm inertia (J_{arm}) couples to the steering wheel (J_s). The muscle co-contraction (intrinsic stiffness, c_{arm}, and damping, k_{arm}) generates the required steering torque, refer (4). Because force/torque is an input to a mechanical system and motion state/s such as position/velocity becomes the feedback. The driver model parameter values are taken from [10]. The motor current controller and sensors (for torsion bar torque and rack position) have fast dynamics. But a first-order transfer function representing their bandwidth ($G_{s,M_{mot}}$, $G_{s,M_{tb}}$ and G_{s,x_r}) is used for the simulation. Their bandwidth are assumed as 2kHz, 1kHz and 1kHz respectively. A time delay of 2ms is also considered from the request to actual EPAS motor torque.

2.2 Steering Feel Reference

This section introduces the reference generator. The given reference model is considered to be a good steering feel representation. It is objectified in terms of torsion bar torque (M_{tb}) to rack position for the existing feed-forward system. For the feedback controller, the derived reference defines the virtual dynamics. The rack motion is controlled in a straightforward manner because both the variables M_{tb} and x_r act on the rack itself. Moreover, the rack dynamics cause the fundamental difference between an electric- and hydraulic-rack assisted steering system. For the analysis, the reference at 75km/h (vehicle speed) is used.

The reference transfer function (5) is proper, since $M_{tb}(s)$ acts as an input and $X_r(s)$ as an output. The two eigenfrequencies represent yaw ($\approx 1-2$Hz) and steering rack ($\approx 2-3$Hz) dynamics. However, the reference inverse (6) is improper and requires a second-order filter (with damping ratio D_f and cut-off frequency ω_f), further discussed below. The requirement of reference inverse and reference is for torque- and position-control (outer loop) respectively, refer Fig. 2.

$$G_{ref} = \frac{X_r(s)}{M_{tb}(s)} = \frac{b_2 s^2 + b_1 s + b_0}{a_4 s^4 + a_3 s^3 + a_2 s^2 + a_1 s + a_0} \quad (5)$$

$$G_{ref}^{-1} = \frac{M_{tb}(s)}{X_r(s)} = \frac{1}{G_{ref}} \frac{\omega_f^2}{s^2 + 2D_f\omega_f s + \omega_f^2} \quad (6)$$

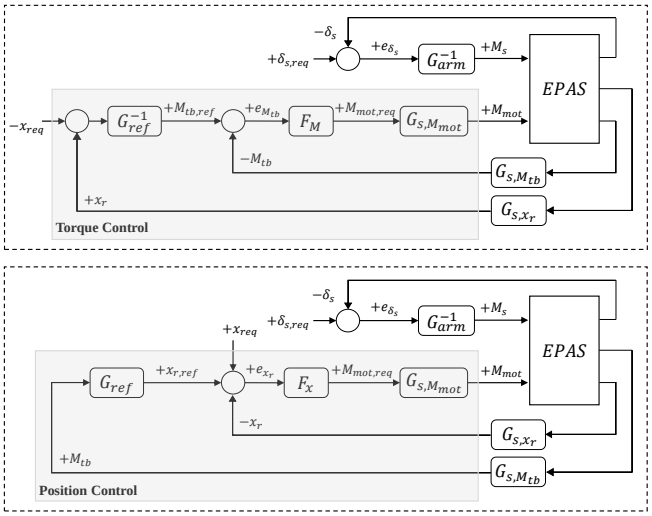

Figure 2: Schematic scheme of the closed-loop steering feedback control strategies in an EPAS system (as the plant); (a) Torque- and (b) Position-control respectively.

2.3 System Identification

Before designing the haptic controller, it is essential to identify the steering rack impedance, i.e., dynamic rack mass (due to EPAS motor inertia), m_r, and viscous damping, k_r. The system identification is performed on the steering test rig. The steering rack is connected to two external linear actuators on each side. Open loop identification is done with freely rotating steering wheel, such that $M_s(t) = 0$.

The parameters m_r, k_r are estimated by exciting one of the linear actuators with a reference force in passive EPAS-Off condition, $M_{mot}(t) = 0$. The external rack force for the selected reference stiffness (c_{ref}) becomes, $F_r(t) = -c_{ref}(x_{r,ref}(t) - x_r(t))$. The LTI transfer function estimate (ratio of output-input cross to input spectrum) is derived from the measurement data. The coherence spectrum criteria, $(\hat{k}_{yu}^N(\omega))^2 \geq 0.95$, is followed for lower noise interference. Neglecting the torsion bar torque disturbance (as a simplified assumption), $M_{tb}(t) \approx 0$. Equation (2) is transformed to Laplace domain resulting in (7), refer Fig. 3 for the frequency response plot. EPAS-On condition signifies the implemented feed-forward algorithm, such that $M_{mot}(t) \neq 0$.

$$H(s) = \frac{X_r(s)}{X_{r,ref}(s)} = \frac{c_{ref}}{m_r s^2 + k_r s + c_{ref}} \quad (7)$$

$$V_n = \frac{1}{n}\sum_{i=1}^{n}\left(1 - \frac{|\hat{H}(j2\pi f_i)|}{|H(j2\pi f_i)|}\right)^2 \quad (8)$$

The cost function (V_n) in (8) uses the estimated ($\hat{H}(j\omega)$) and fitted ($H(j\omega)$) frequency response magnitude at selected frequencies for error minimization (by linear least squares criterion). The optimization result (in EPAS-Off) gives steering rack impedance parameters. However in reality, the inertia of the front wheels is also added to the steering rack mass. Here it is done afterwards, considering a static steering arm (or linkage) ratio.

2.4 Problem Formulation

This paper highlight key differences between the closed-loop methods for compensating the steering rack impedance (due to EPAS motor). As stated before, the controllers are developed in a sequential manner with a defined stability criteria using classical methods. The stability conditions at each step of the design procedure are mathematically derived. This provides a quantified comparison between the feedback control solutions. Secondly, the disturbance rejection is evaluated for the same control law. Finally the issue of merging the external rack position request (in hands-on/off situations) is addressed for the controllers.

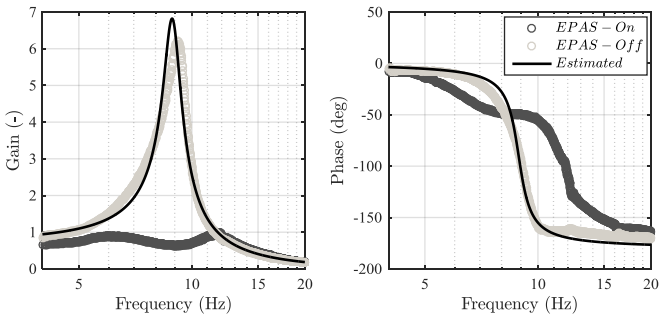

Figure 3: System identification result from the steering test rig. Frequency response of reference to actual rack position, $H(j\omega)$, for conditions EPAS-On and -Off respectively. Also, an estimated second-order system with identified passive steering rack mass, m_r, and viscous damping, k_r.

3 HAPTIC FEEDBACK CONTROL

The feedback control objective is to track the reference by compensating the rack impedance. The design methodology for the closed-loop possibilities is discussed in this section. For the final (numerical and simulation) results, the rack force is considered to be given by a single-track vehicle model. However for simplicity, the analytical expressions in the following equations is achieved considering the rack stiffness (c_r), such that the rack force becomes, $F_r(t) = c_r x_r(t)$. The combined EPAS system and vehicle model is called the plant, see Fig. 2. The plant model has different parameters (such as tire cornering stiffness, yaw inertia, etc.) as compared to the reference. The controller is designed in a stepwise manner; coupling of the feedback control to the plant, coupling the reference/reference inverse and human/driver coupling. The worst-case scenario is assumed for the controller design, rigidly coupled driver arm inertia to the steering wheel with high muscular arm stiffness. The phase margin at each step has been evaluated and the gain margin is fixed to infinite. For a robust performance, the phase margin of each loop gain is set between $30^\circ - 60^\circ$ [11]. In simulation, the controller stability was maintained at all times and the EPAS motor torque never exceeded its saturation limit (5Nm).

3.1 Torque Control

This architecture requires reference inverse in the outer loop and torque feedback in the inner loop as shown in Fig. 2(a). The strategy is termed on the basis of feedback control variable (i.e. torsion bar torque). The reference torque (9) is requested to the feedback control, which results in (10) for the motor torque.

$$M_{tb,ref}(s) = G_{ref}^{-1} X_r(s) \tag{9}$$

$$M_{mot}(s) = F_M(M_{tb,ref}(s) - M_{tb}(s)) \tag{10}$$

Using (2) and above mentioned equations, the tracking and reference transfer functions are given as (11) and (12) respectively. Consider a proportional feedback, $F_M = -K_{p,M}$, without the outer loop. As a result, the steering rack impedance in (11) is reduced by a factor of $(1 + K_{p,M} i_{epas})$, where $i_{epas} = i_{mot}/i_{rp}$ and $K_{p,M} > 0$. This can also be proved using the initial value theorem on (12) for a given (simplified) reference inverse in (13). Therefore, the requirement of proportional gain in torque-control for the given plant is essential to overcome the mechanical impedance. This is necessary to compensate the motor inertia.

$$\frac{X_r(s)}{M_{tb}(s)} = \frac{i_{rp} - F_M i_{mot}}{(m_r s^2 + k_r s + c_r) - G_{ref}^{-1} F_M i_{mot}} \tag{11}$$

$$\frac{M_{tb}(s)}{M_{tb,ref}(s)} = \frac{(m_r s^2 + k_r s + c_r) - G_{ref}^{-1} F_M i_{mot}}{G_{ref}^{-1}(i_{rp} - F_M i_{mot})} \tag{12}$$

$$G_{ref}^{-1} = (m_{ref} s^2 + k_{ref} s + c_{ref})/i_{rp} \tag{13}$$

The integral part is required for reference tracking. This is proved using the final value theorem on (11) which shows the steady state error. Considering $F_M = -K_{i,M}/s$, a step disturbance in rack position, Δx_r, at $t = 0$ results in steady state torque, ΔM_{tb}, as shown in (14). For minimum stationary error at lower frequencies, $K_{i,M}$ (> 0) should be large.The quantification of $K_{p,M}$ and $K_{i,M}$ is explained under stability analysis.

$$\Delta M_{tb} = \lim_{s\to 0} \frac{M_{tb}(s)}{X_r(s)} \Delta x_r = \lim_{s\to 0} \left[\frac{c_{ref} + \frac{c_r s}{K_{i,M} i_{epas}}}{1 + \frac{s}{K_{i,M} i_{epas}}} \right] \frac{\Delta x_r}{i_{rp}} \tag{14}$$

The ideal torque-control law should consist of proportional and integral gains as defined in (15). The feedback control is designed such that it is independent of reference/reference inverse with high inner loop bandwidth. The open loop transfer function from motor torque to torsion bar torque (obtained from (1)−(3) in Laplace domain) has a zero at the origin. Using the integral feedback gain results in a pole/zero cancellation. Despite that, the closed-loop LTI system remains reachable and observable (for rack position on the outer loop).

$$F_M = -(K_{i,M}/s + K_{p,M}) \tag{15}$$

The stability property of the inner loop is investigated at first. The inner loop gain becomes (16) with control law (15). Open transfer function signifies the (open loop) plant behavior using (1)−(3). The feedback controller governs the inner loop stability. Higher $K_{p,M}$ ensures lower mechanical impedance and higher (inner loop gain) phase margin; whereas higher $K_{i,M}$ is required for reference tracking but at the cost of a reduced phase margin. The constraint (17) must be satisfied for the inner loop stability as a necessary and sufficient condition. For a given $K_{p,M}$, $K_{i,M}$ has an upper bound limiting the tracking performance. This has been analytically derived (and numerically verified) by neglecting the small terms with respect to high torsion bar stiffness as an assumption. With reducing stiffness, the upper bound increases. Increasing $K_{p,M}$ gives a higher upper bound on $K_{i,M}$. But $K_{p,M}$ is also limited by the time delay in motor torque request for stability. $K_{i,M}$ upper bound is primarily dependent on $K_{p,M}$, m_r and k_{tb}. Although it is somewhat dependent on the driver arm inertia (J_{arm}), but the inner loop performance (in terms of bandwidth) is not compromised as seen in Fig. 4(a). Hence, the inner loop (controller) performance is almost insensitive to J_{arm} variation. Lower torque sensor bandwidth reduces the phase margin, which is undesirable for stability and robustness.

$$L_{in,M} = F_M \left| \frac{M_{tb}(s)}{M_{mot}(s)} \right|_{open} \tag{16}$$

$$K_{i,M} < \frac{1}{i_{epas}} \left[\frac{(\alpha k_{tb} + \frac{k_r}{i_{rp}^2})(\alpha + \frac{c_r}{c_{tb} i_{rp}^2})}{m_r/i_{rp}^2} + \frac{2\alpha k_{tb}}{J_s + J_{arm}} + \right. \tag{17}$$

$$\left. + \frac{(b_s + k_{tb}) m_r / i_{rp}^2}{(J_s + J_{arm})^2} \right];\ where,\ \alpha = 1 + K_{p,M} i_{epas}$$

The next step is to integrate the reference inverse on the outer loop. The resulting loop gain is shown in (18). There are two possibilities for the integration; either the feedback control is given and the reference inverse needs to be designed or vice versa. The reference impedance parameters, m_{ref} and k_{ref}, do not affect the stability. But the reference stiffness, c_{ref}, limits the outer loop performance. At first, consider a torque controller to be given with a bandwidth, ω_{in}, such that $T_s = 1/\omega_{in}$. The valid (non-negative) solution of the quadratic equation (19) gives the upper bound on c_{ref}. But if the inequity constraint (20) holds true, then the outer loop is stable $\forall\ c_{ref} > 0$. In the second possibility (focus of the paper), the outer loop is stable $\forall\ c_{ref} > 0$, if the constraint (21) holds. Typically $c_{ref} < c_r$, because the purpose of EPAS is to reduce the plant stiffness (or steering effort). m_{ref} and k_{ref} are implemented as feed-forward (with a suitable

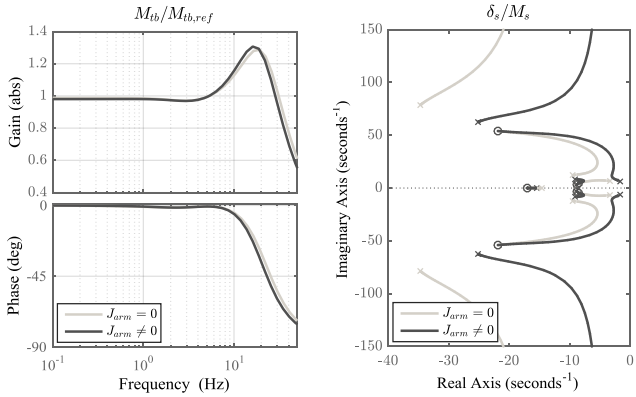

Figure 4: Torque feedback control. (a) Analytical inner loop frequency response without and with driver arm inertia. (b) Root locus plot for the driver admittance (δ_s/M_s) with muscular arm stiffness (c_{arm}) variation.

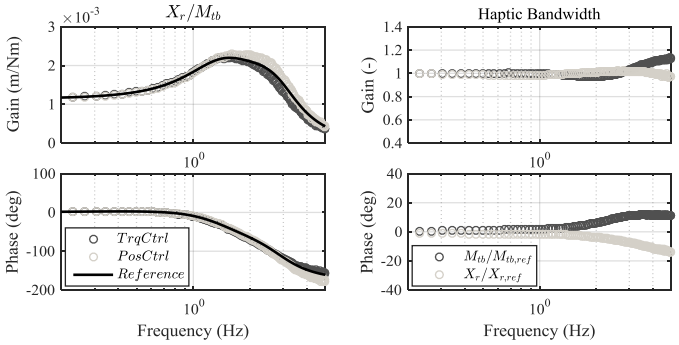

Figure 5: Simulation result: (a) Frequency response of torsion bar torque to steering rack position for torque- and position-control in comparison to reference. (b) The haptic bandwidth is defined in terms of reference transfer function (Torque control $-M_{tb}/M_{tb,ref}$ and Position control $-X_r/X_{r,ref}$).

filter) in the reference inverse. The inverse filter time constant ($T_f = 1/\omega_f$) should be low for a good tracking performance. On the contrary, it is constrained by the controller sampling rate to prevent numerical instability. For the given reference inverse, $T_f = 5$ms with critical damping ratio, $D_f = 0.707$, provides 60° phase margin for (18).

$$L_{o,M} = F_M \left[\left| \frac{M_{tb}(s)}{M_{mot}(s)} \right|_{open} - G_{ref}^{-1} \left| \frac{X_r(s)}{M_{mot}(s)} \right|_{open} \right] \quad (18)$$

$$c_{ref}^2 \quad + \quad c_{tb} i_{rp}^2 \left(2 + \frac{b_s T_s}{J_s + J_{arm}} - \frac{c_{tb} T_s}{b_s} \right) c_{ref} + \quad (19)$$

$$+ \quad \left(1 + \frac{b_s T_s}{J_s + J_{arm}} \right) (c_{tb} i_{rp}^2)^2 > 0$$

$$\omega_{in} > \left(c_{tb} - b_s^2/(J_s + J_{arm}) \right)^2 / 4 b_s c_{tb} \quad (20)$$

$$K_{i,M} < K_{p,M} \left(k_r + (1 + K_{p,M} i_{epas}) k_{tb} i_{rp}^2 \right) / m_r \quad (21)$$

$$L_s = G_{arm}^{-1} \left| \frac{\delta_s(s)}{M_s(s)} \right|_{closed} \quad (22)$$

Finally stability of the torque controller depends on its interaction with the driver. Coupled instability of haptic controllers during human interaction is a common phenomenon [12]. The driver admittance is defined as the ratio of steering angle to torque, δ_s/M_s, which represents the human interaction. Coupled stability depends on J_{arm} and c_{arm}. The inner loop maintains the required stability and performance irrespective of varying J_{arm} satisfying constraint (17). The effect of muscle co-contraction is understood using the root locus plot. For this, the loop gain of the closed-loop system is (22), where $G_{arm}^{-1} = c_{arm} + k_{arm} s$, as derived from (4). Following this stepwise controller design approach, the closed-loop admittance ensures a stable human coupling. It is evident from the admittance root locus plot as shown in Fig. 4(b). With increasing c_{arm}, the poles (especially the dominant one defined by J_{arm}) stay in LHP.

The controller is designed analytically at first and then verified in simulation. The controller bandwidth is approximately 20Hz (for rigidly coupled hands-on situation). With reducing J_{arm}, it remains almost same. The simulation result can be seen in Fig. 5(a). The reference tracking of torsion bar torque to rack position is well matched. The haptic bandwidth (defined by the ratio of reference to actual control variable) stays close to 1 within the driver's steering excitation range as shown in Fig. 5(b).

3.2 Position Control

The position-control approach has reference (5) in the outer loop and position feedback in the inner loop as shown in Fig. 2(b). The reference steering rack position is derived using the torsion bar torque as (23). The resulting motor torque request is given in (24). Considering (2), the (position-control) tracking and reference transfer functions are given as (25) and (26) respectively.

$$X_{r,ref}(s) = G_{ref} M_{tb}(s) \quad (23)$$

$$M_{mot}(s) = F_x (X_{r,ref}(s) - X_r(s)) \quad (24)$$

$$\frac{X_r(s)}{M_{tb}(s)} = \frac{i_{rp} + G_{ref} F_x i_{mot}}{(m_r s^2 + k_r s + c_r) + F_x i_{mot}} \quad (25)$$

$$\frac{X_r(s)}{X_{r,ref}(s)} = \frac{i_{rp} + G_{ref} F_x i_{mot}}{G_{ref}((m_r s^2 + k_r s + c_r) + F_x i_{mot})} \quad (26)$$

The position feedback control (F_x) is derived using the torque feedback control law, F_M. The criteria is to place the closed-loop poles at the same location in the complex plane. This implies same characteristic equation ($G_{char} = 1 + L_o$) for the closed-loop plant. The final result is shown in (27). For manipulating the haptic feedback (torque) using the position-control method, the inner loop requires a higher order transfer function to reduce the error in steering rack speed and acceleration. This is motivated in (28), as derived from (13) and (27). The resulting feedback control law becomes (29) using (15). The feedback controller gains ($K_{d2,x}, K_{d,x}, K_{p,x}, K_{i,x}$) should be quantified independent of reference parameters. For practical reasons, the derivative and double-derivative terms require filtering. With this, the closed-loop LTI system is reachable and observable since no pole/zero cancellations takes place.

$$G_{char,M} \stackrel{!}{=} G_{char,x} \implies F_x = -F_M G_{ref}^{-1} \quad (27)$$

$$F_x = -F_M (m_{ref} s^2 + k_{ref} s + c_{ref}) / i_{rp} \quad (28)$$

$$F_x = K_{d2,x} s^2 + K_{d,x} s + K_{p,x} + K_{i,x}/s \quad (29)$$

The requirement of each feedback gain is discussed next. It is done by developing the inner loop for the steering rack as the plant defined by (2). $M_{tb}(t)$ is considered as an external disturbance (rather than a state variable). The resulting closed-loop reference and disturbance transfer functions are (30) and (31) respectively. Introducing the proportional gain, $K_{p,x} > 0$, adjusts the reference bandwidth. Higher gain is desirable but it reduces the damping ratio (and phase margin). The addition of the derivative part ($K_{d,x} > 0$) compensates for it. However, the derivative filter (with time constant T_f) has limitations. For a certain $K_{p,x}$ and $T_f = 5$ms, $K_{d,x}$ is selected to achieve 60° inner loop gain phase margin. Further increase in $K_{d,x}$ reduces the phase margin. The integral gain, $K_{i,x}$, ensures lower steady-state and integrated error for a position request and load-torque disturbance respectively. This is proved using the final value theorem on (31) to compute the integrated position error. For a step torque disturbance, ΔM_{tb}, at $t = 0$ the integral position error is given by (32). As $K_{i,x}$ increases, the integrated error decreases. Since the

proportional gain in torque-control compensates the mechanical impedance, the double-derivative gain ($K_{d2,x}$) in position-control fulfills that purpose. The initial value theorem on (30) proves this claim as shown in (33) for a step position request, $\Delta x_{r,ref}$, at $t = 0$. Higher $K_{d2,x}$ is desirable to overcome the rack mass (which is a primary motive), but the phase margin limits the upper bound due to the second-order derivative filter. Another important reason for smaller $K_{d2,x}$ is that the double-derivative amplifies the sensor noise incredibly. The torque-control filter for reference inverse is used here for an unbiased comparison between the two methods. The quantification of $K_{i,x}$ and $K_{d2,x}$ is explained in the stability part.

$$\frac{X_r(s)}{X_{r,ref}(s)} = \frac{F_x i_{mot}}{m_r s^2 + k_r s + c_r + F_x i_{mot}} \tag{30}$$

$$\frac{X_r(s)}{M_{tb}(s)} = \frac{i_{rp}}{m_r s^2 + k_r s + c_r + F_x i_{mot}} \tag{31}$$

$$\lim_{t\to\infty} \int_0^t \Delta x_r dt = \lim_{s\to 0} \frac{X_r(s)}{M_{tb}(s)} \frac{\Delta M_{tb}}{s} = \frac{\Delta M_{tb}}{K_{i,x} i_{epas}} \tag{32}$$

$$\Delta x_r = \lim_{s\to\infty} \frac{X_r(s)}{X_{r,ref}(s)} \Delta x_{r,ref} = \frac{\Delta x_{r,ref}}{1 + \frac{m_r}{K_{d2,x} i_{mot}}} \tag{33}$$

The feedback control is coupled to the plant for the inner loop. The stability is defined by the loop gain (34). $K_{i,x}$ defines the stiffness of the closed-loop position-control plant, whereas $K_{d2,x}$ represents the dynamics. To ensure stability of the inner loop, (35) must be satisfied (necessary and sufficient condition). This analytical result does not include controller derivative filter for simplicity. There are two key aspects for the constraint. For a given $K_{d2,x}$, there exists an upper bound on $K_{i,x}$ or vice versa. Ideally both the gains should be higher but the constraint limits the inner loop performance. Increasing $K_{d2,x}$, lowers $K_{i,x}$ upper bound. This is contrary to the torque-control constraint in (17). Also, higher m_r or J_{arm} limits the inner loop performance and stability margin such that the upper bound on either $K_{i,x}$ or $K_{d2,x}$ decreases noticeably. As seen in Fig. 6(a), the inner loop bandwidth changes with and without J_{arm} keeping the same feedback control. As a consequence, the position-control inner loop phase margin is set higher than torque-control because of its sensitivity towards varying J_{arm}.

$$L_{in,x} = F_x \left| \frac{X_r(s)}{M_{mot}(s)} \right|_{open} \tag{34}$$

$$K_{i,x} < \left[\frac{b_s + \left(\frac{k_r + K_{d,x} i_{mot}}{i_{rp}^2}\right)}{J_s + J_{arm} + \left(\frac{m_r + K_{d2,x} i_{mot}}{i_{rp}^2}\right)} \right] \left[\frac{c_r}{i_{mot}} + K_{p,x} \right] \tag{35}$$

In the next step, the reference is introduced on the outer loop and coupled to the position controlled plant. The loop gain is given as (36). Considering the two possibilities for the inner and outer loop integration. In the first case, the choice of reference admittance parameters k_{ref} and c_{ref} does not affect the controller stability for a given feedback control. But the admittance mass, m_{ref}, cause the limitation because it defines the reference dynamics. With an inner loop bandwidth (ω_{in}) defined by the feedback control, m_{ref} lower bound is given as (37) such that $T_s = 1/\omega_{in}$. It is possible to have fast reference dynamics (which implies lower m_{ref}) either by decreasing the inertia ($J_s + J_{arm}$) or increasing ω_{in}. However, the inner loop bandwidth is also dependent on the inertia as shown above. The other possibility is feedback control design for a given reference. The stability holds, if the lower bound condition on $K_{d,x}$ obtained by solving (38) is fulfilled. The simplified resulting constraint primarily depends on the system inertia and m_{ref}. For lower m_{ref} and higher J_{arm} or m_r, $K_{d,x}$ lower bound increases for the outer loop stability. This is in conflict with phase margin. Because as $K_{d,x}$ increases, the inner loop gain phase margin decreases.

$$L_{o,x} = F_x \left[\left| \frac{X_r(s)}{M_{mot}(s)} \right|_{open} - G_{ref} \left| \frac{M_{tb}(s)}{M_{mot}(s)} \right|_{open} \right] \tag{36}$$

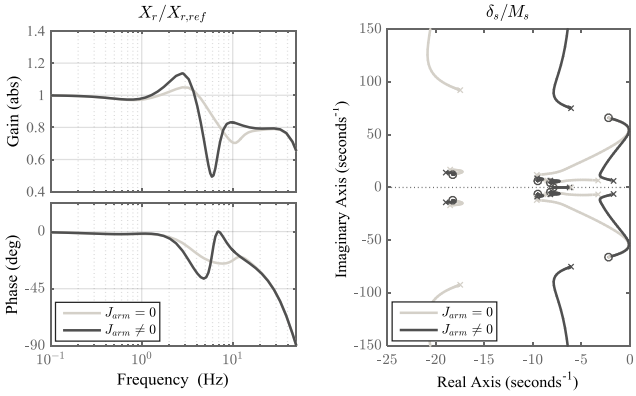

Figure 6: Position feedback control. (a) Analytical inner loop frequency response without and with driver arm inertia. (b) Root locus plot for the driver admittance (δ_s/M_s) with muscular arm stiffness (c_{arm}) variation.

$$m_{ref} > \frac{J_s + J_{arm}}{(b_s + k_{tb})/i_{rp}^2} \left[\frac{\left(c_{tb} - \frac{k_{tb}^2}{J_s + J_{arm}}\right) T_s - k_{tb}}{1 + \frac{b_s + k_{tb}}{J_s + J_{arm}} T_s + \frac{c_{tb}}{J_s + J_{arm}} T_s^2} \right] \tag{37}$$

$$K_{d,x}^2 + \frac{1}{i_{mot}} \left[\frac{-\left(\frac{m_r}{m_{ref}} - 1\right) c_{tb}}{\left(\frac{1/i_{rp}^2}{J_s + J_{arm}} + \frac{1}{m_{ref}}\right) k_{tb}} + k_{tb} \left(i_{rp}^2 + \frac{m_r}{J_s + J_{arm}} \right) \right] K_{d,x} + \frac{\frac{c_{tb}}{i_{mot}^2} \left(\frac{m_r}{J_s + J_{arm}} + i_{rp}^2\right)^2}{\left(\frac{1}{J_s + J_{arm}} + \frac{i_{rp}^2}{m_{ref}}\right)} > 0 \tag{38}$$

The effect of muscle co-contraction is analytically explained using (22) as the loop gain for the coupled interactions. If the above constraints hold true, then the closed-loop admittance could be made stable independent of c_{arm}. This ensures contact stability for human coupled interactions in position controlled systems [12, 6]. Fig. 6(b) presents the driver admittance root locus plot for the muscle co-contraction level. With increasing c_{arm}, the closed-loop admittance poles remain in LHP. The dominant pole defined by J_{arm} (although stays in LHP) move towards the $j\omega-$axis (marginal stability) with increasing gain. This would cause contact instability, if the haptic position controller is not designed properly. Hence, this method is not only sensitive to J_{arm} variation but to the muscle co-contraction as well, especially if the plant has high inertia or m_r.

The haptic position controller bandwidth is defined by the inner loop. For generic parameters, the bandwidth achieved is approximately 11Hz and 6Hz without and with driver-in-the-loop (or J_{arm}) respectively. The reference tracking from simulation result can be seen in Fig. 5(a). Frequency response of torsion bar torque to rack position is similar to torque-control with some deviations at higher frequencies due to filtering of the higher order derivative/s in the inner loop. The haptic control variable (function) is shown in Fig. 5(b), which stays close to 1 as desired.

3.3 Road Disturbance Attenuation

After a similar tracking performance for haptic controllers, the next point of comparison is disturbance rejection with their respective control law. This is obtained by grounding $\delta_{s,req}$ ($= 0$) and adding an external road input ($F_{r,dist}$) on the steering rack, see Fig. 1. The resulting disturbance attenuation (closed-loop) frequency response is shown in Fig. 7(a). For low frequency disturbances (< 1Hz), torque-control has better attenuation. Because the steering rack stiffness is high and the torque controller performs better with stiffer environments as mentioned in [13]. For high frequencies (> 5Hz), torque-control again provides more disturbance rejection than position-control. Higher arm inertia is desirable for high frequency noise attenuation. But position-control (with $J_{arm} \neq 0$) shows less damping around

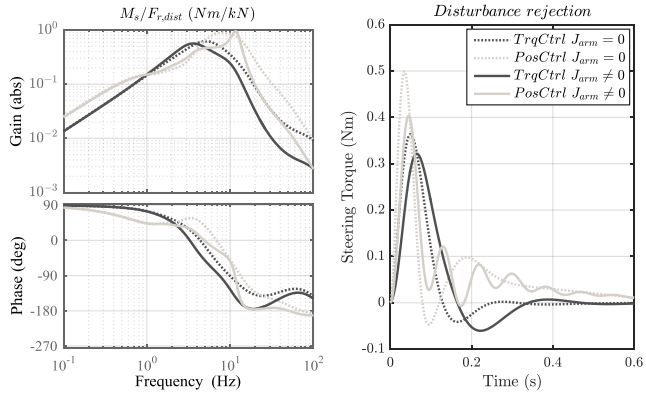

Figure 7: Disturbance rejection. Dark and light gray lines are torque/position-control respectively. Solid and dotted lines are with and without J_{arm} respectively. (a) $M_s/F_{r,dist}$ closed-loop frequency response. (b) Step response of M_s for $F_{r,dist} = 1$kN.

10Hz at the steering wheel eigenfrequency due to increase in system inertia and limited feedback control performance. Subsequently, the oscillations in position-control steering torque response for a disturbance step, $F_{r,dist} = 1$kN, can be seen in Fig. 7(b). High system inertia causes limitation in position-control for high frequency disturbance rejection. This requires further improvement in the feedback control especially for the higher order derivative/s to control high system inertia. Within mid-frequency range $(1 - 5$Hz), the steering rack stiffness (which is a function of front axle lateral slip) drops and the position controller offers better attenuation for softer environments, see [13]. The controller performance is closely matched analytically. Hence, they will be compared in reality both objectively and subjectively as next steps.

4 MERGING LATERAL CONTROL REQUEST

Lateral vehicle control functions are based on steering rack position request. As shown in Fig. 2, the external request can be added directly to the inner loop before the feedback control in the position controller as a straightforward solution. In case of torque-control, the position request is subtracted from the actual rack position in the outer loop before the reference inverse. Both methods provide a comparable performance in hands-on/off conditions with a bandwidth 1.5Hz and similar stability margin. This external intervention performance is only sufficient for low frequency requests, e.g. in Lane Keeping Aid, etc. Higher bandwidth might be achievable with other controller layouts, but it would require additional tuning.

5 CONCLUSIONS

In this paper, the closed-loop haptic feedback control methods for an EPAS system are investigated. The objective is to compensate the motor impedance on the steering rack and track the desired reference defining the steering feel. In torque-control, the proportional gain is necessary to overcome the mechanical rack impedance. Whereas in position-control, the double-derivative term fulfills the same purpose. The higher order derivatives in position feedback control (with suitable filtering) are required to overcome the inertia and achieve an acceptable reference tracking. As a consequence of the filtering and stability constraint, the position-control inner loop bandwidth is limited. Increasing the system inertia hampers stability and high frequency tracking. Moreover, increasing the driver arm inertia further deteriorates the position-control inner loop stability and performance. On the contrary, the torque-control inner loop is almost insensitive to the arm inertia variation. However, the torque-control outer loop limits the reference tracking due to filtering without causing controller stability issues. For human coupled interactions, the position controller is more sensitive to the muscle co-contraction. Following the controller design procedure outlined in the paper, it is possible to realize a similar reference tracking performance (within the driver's steering excitation range) and stability margin in both the cases. Subsequently, the resulting torque controller haptic bandwidth is higher than the position controller.

For road disturbance attenuation, the torque controller offers better performance in low frequency range due to higher system stiffness. As the stiffness reduces with increasing frequency, the position controller performs better (for mid-frequency range). However at higher frequencies, the position feedback control has limited performance due to high system inertia. As a result, the torque controller provides higher attenuation. For external rack position request, the controllers have similar performance in both hands-on/off conditions. Experiments in vehicle will be performed to evaluate the steering feel and external lateral vehicle control intervention for the controllers under different conditions and driver excitations.

ACKNOWLEDGMENT

The research activities are performed as a part of the ITEAM project in the European Union's Horizon 2020 research and innovation program under Marie Sklodowska-Curie Grant Agreement No. 675999. The authors would like to thank Professor Bengt Jacobson from Chalmers University of Technology and Pontus Carlsson from Volvo Cars for their technical support.

REFERENCES

[1] Aguirre-Ollinger, G. et al. "Inertia Compensation Control of a One-Degree-of-Freedom Exoskeleton for Lower-Limb Assistance: Initial Experiments." In: *IEEE Trans. Neural Syst. and Rehab. Engg.* 20 (2012), pp. 68–77.

[2] Harrer, M. and Pfeffer, P. *Steering Handbook.* Switzerland: Springer International Publishing AG, 2017, pp. 178–189, 456–466.

[3] Chugh, T. et al. "Design and control of model based steering feel reference in an electric power assisted steering system." In: *25th IAVSD Symposium* (2017), pp. 43–48.

[4] Brocker, M. "New control algorithms for steering feel improvements of an electric powered steering system with belt drive." In: *Veh. Syst. Dyn.* 44.1 (2006), pp. 759–769.

[5] Skogestad, S. and Postlethwaite, I. *Multivariable Feedback Control: Analysis and design.* 2001, pp. 194–200.

[6] Schouten, A. C. et al. "Design of a torque-controlled manipulator to analyse the admittance of the wrist joint." In: *Jornal of Neurosci. Methods* 154 (2006), pp. 134–141.

[7] Dannöhl, C., Müller, S., and Ulbrich, H. "H∞-control of a rack-assisted electric power steering system." In: *Veh. Syst. Dyn.* 50:4 (2012), pp. 527–544.

[8] *Pilot Assist.* `https://www.volvocars.com/us/cars/new-models/s90`. Accessed: 2018-05-12.

[9] Rajamani, R. *Vehicle Dynamics and Control.* Spring International, 2012, pp. 27–40.

[10] Cole, D. J. "A path-following driver-vehicle model with neuromuscular dynamics, including measured and simulated responses to a step in steering angle overlay." In: *Veh. Syst. Dyn.* 50:4 (2012), pp. 573–596.

[11] Åström, K. J. and Murray, R. M. *Feedback Systems - An Introduction for Scientists and Engineers.* Princeton and Oxford: Princeton University Press, 2009, pp. 251–252.

[12] Colgate, J. E. "Robust control of dynamically interacting systems." In: *Int. Journal of Cont.* 48.1 (1988), pp. 65–88.

[13] Ott, C., Mukherjee, R., and Nakamura, Y. "Unified impedance and admittance control". In: *IEEE Int. Conf. Rob. and Aut.* (2010), pp. 554–561.